ACS OMEGA

Open Access

http://pubs.acs.org/journal/acsodf

Article

Synergistic Effect of Amino-Modified Co-MOF and APP on Improvement of the Fire Safety of the Rigid Polyurethane Foam

Zijin Chen, Shujie Yuan,* and Xiaoxue Xu

Cite This: *ACS Omega* 2025, 10, 892−903

Read Online

ACCESS | Metrics & More | Article Recommendations

ABSTRACT: The combustion of rigid polyurethane foam (RPUF) generates significant amounts of toxic and high-temperature smoke, which restricts its application. Here, an amino-modified Co-MOF (NH_2−Co-MOF) was synthesized and it was used in conjunction with ammonium polyphosphate (APP) to decrease the flammability of RPUF. We obtained the expected results: the fire safety of RPUF was greatly enhanced by the addition of NH_2−Co-MOF and APP. Compared to neat RPUF, the peak heat release rate (pHRR) and total heat release (THR) values of N−C/A/RPUF decreased by 22.5 and 37.4%, respectively. Based on the analysis of combustion products of the gaseous and condensed phases, it can be seen that the synergistic use of NH_2−Co-MOF with APP enhances the barrier effect, dilutes combustible gases, and quenches the combustion chain reaction.

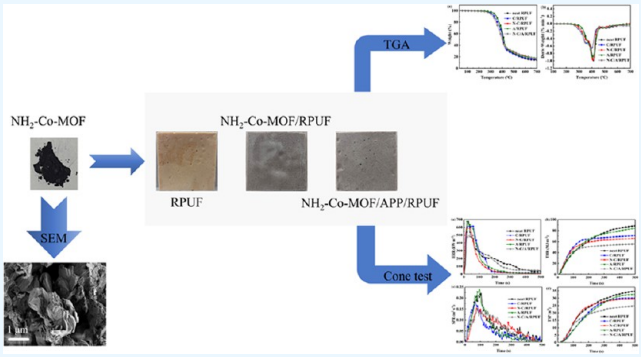

1. INTRODUCTION

The rigid polyurethane foam (RPUF) is a solid foam formed by the reaction of polyol and isocyanate liquid components with the aid of a foaming agent and catalyst.[1,2] RPUF is a low thermal conductivity material known for its high strength and outstanding thermal insulation properties, usually utilized in construction, transportation, and aviation.[3−6] However, its cellular structure and organic components make it highly susceptible to combustion at high temperatures or flames.[7,8] Moreover, the combustion of RPUF can lead to the generation of toxic and harmful smoke such as carbon monoxide (CO), nitrogen oxides (NO_X), and cyanide (HCN).[9] Therefore, how to improve the fire safety of RPUF has become a significant issue that urgently needs to be solved.[10]

Typically, the common method to decrease the flammability of RPUF involves incorporating flame retardants or reactive flame retardants.[11] The reactive flame retardancy of RPUF is often achieved by flame retardant modification of polyols, like melamine-based polyether polyols,[12] and phosphorus containing and nitrogen-containing polyols.[13] However, the reactive flame retardancy of RPUF struggles to satisfy the fire resistance requirements of building materials. In contrast, adding flame retardants is more convenient and widely used. Under the requirement of green and halogen-free, ammonium polyphosphate (APP)[14] and melamine polyphosphate (MPP)[15] are common phosphorus-based flame retardant additives used to improve RPUF fire safety. Additionally, nitrogenated flame retardants such as melamine cyanurate (MC) and guanidine phosphate (GP) are often used to decrease the flammability of RPUF. Although these additives significantly enhance the fire safety of RPUF, the substantial amounts required may lead to a notable reduction in the thermal insulation or mechanical properties of RPUF. In order to ensure the other properties of RPUF, people have started to use nanomaterials as flame retardants to improve the combustion behavior of RPUF. Nanomaterials such as layered double hydroxides (LDHs)[16] and graphene oxide (GO)[17] have a positive effect on improving the combustion behavior of RPUF.

Metal organic frameworks (MOFs) exhibit promising application prospects in various fields, including gas storage, catalysis, sensing, and drug delivery.[18−20] MOFs consist of both organic and inorganic components that can decrease the flammability of polymers, offering significant advantages in terms of structure and composition.[21−23] Research has shown that the Zeolitic imidazolate frameworks (ZIFs) are the most commonly used MOF as a flame retardant additive.[24,25] Hou et al.[26] prepared Co-MOF and Fe-MOF and used them as flame retardants for polystyrene (PS). Based on the results, the peak heat release rate (pHRR) values of PS composites-added Fe-MOF and Co-MOF decreased by 14 and 28%, respectively,

Received: August 31, 2024
Revised: December 12, 2024
Accepted: December 19, 2024
Published: December 27, 2024

Table 1. Formulations of Neat RPUF and Flame-Retarded RPUF Composites

sample code	polyether polyol/g	MDI/g	Co-MOF/g	NH_2-Co-MOF/g	APP/g
neat RPUF	20	15			
C/RPUF	20	15	1.0		
N−C/RPUF	20	15		1.0	
A/RPUF	20	15			1.0
N−C/A/RPUF	20	15		0.5	0.5

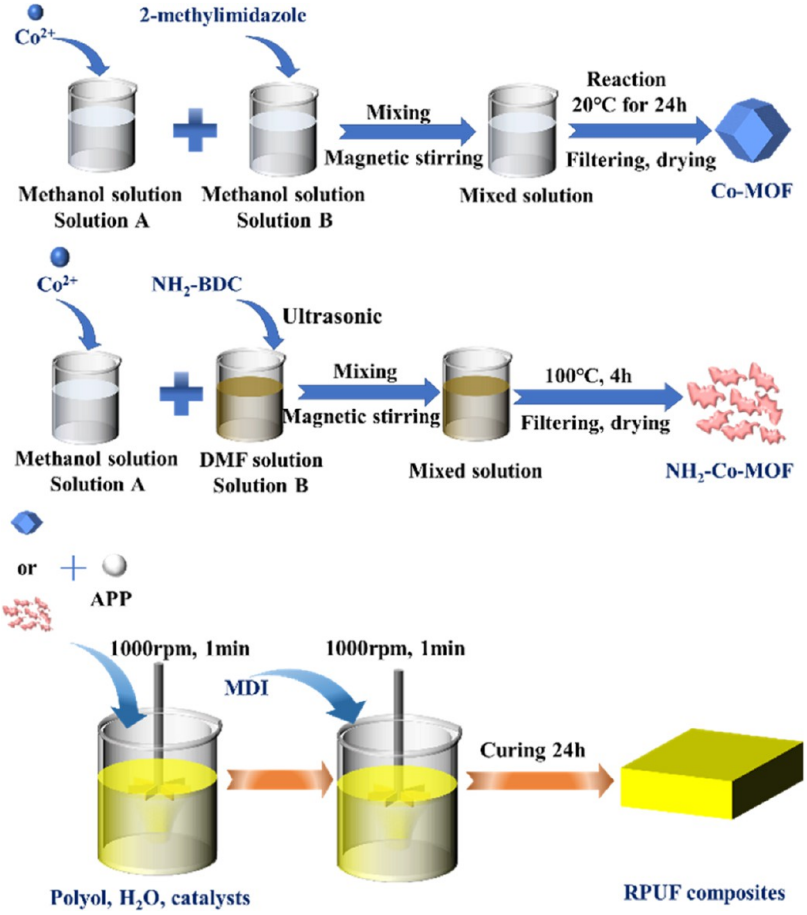

Figure 1. Synthesis scheme of MOFs and RPUF composites.

and the performance of cobalt-containing PS composite is superior to that of iron-containing PS composite. Xu et al.[27] combined water-soluble phenolic resin and ZIF-67 on flexible polyurethane foam (FPUF) surfaces through electrostatic interactions. The coating greatly reduces the emission of toxic gaseous products. Li et al.[28] prepared ZIF-8 (Zn) to add to epoxy resin (EP) as a flame retardant. Research has shown that the addition of ZIF-8 reduces the value of pHRR of composites by 22.7% and the value of total heat release (THR) decreased by 26.8%. Besides, the carbon production rate of composites had increased from 11.3 to 12.3%. In addition to using ZIFs as flame retardants, researchers have also used other MOFs such as the University of Oslo (UiOs) and Materials of Institute Lavoisier frameworks (MILs) as flame retardants. Chen et al.[29] synthesized Zr-MOF (UiO-66) and utilized it to reduce the flammability of PS. According to the results, the values of pHRR and THR of PS/UiO-66 decreased by 26.8 and 14.7%, respectively. In addition, when 5% UiO-66 is added, the value of total smoke production (TSP) decreased by more than 35%.

In recent years, ZIF has started to be regarded as a flame retardant additive, aiming to enhance the fire safety of RPUF. Cheng et al.[30] prepared RPUF flame retardant composites using three types of ZIFs (ZIF-7/RPUF, ZIF-8/RPUF, ZIF-11/RPUF) and compared the flame retardancy of the three composites. The results showed that the addition of ZIFs improved the flame retardancy of the composites. Among them, the pHRR and THR values of ZIF-8/RPUF reached their lowest, which are 489.56 $kW·m^{-2}$ and 28.40 $MJ·m^{-2}$, respectively. Liu et al.[31] used biomass dopamine (PDA) to connect ammonium polyphosphate (APP) and ZIF-67 to prepare a ternary organic−inorganic hybrid flame retardant (A@P-Z) to decrease the flammability of RPUF. The addition of A@P-Z resulted in a 28.6% decrease in the pHRR value. In addition, the COP decreased by 38.1%.

In this study, Co-MOF and amino-modified Co-MOF (NH_2−Co-MOF) were prepared and used as flame retardant additives to prepare RPUF composites (C/RPUF, N−C/RPUF). In addition, NH_2−Co-MOF and ammonium polyphosphate (APP) were physically blended into RPUF (N−C/

https://doi.org/10.1021/acsomega.4c08026
ACS Omega 2025, 10, 892−903

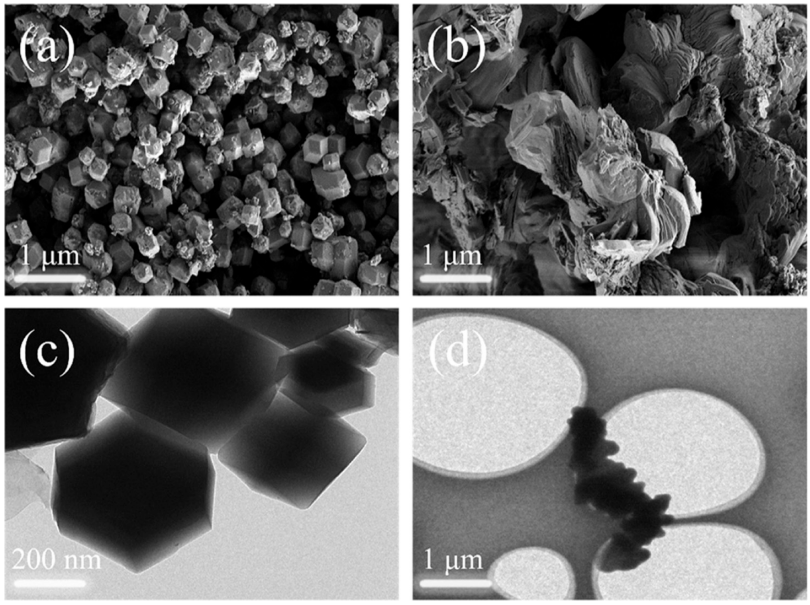

Figure 2. SEM and TEM images of the MOFs. SEM (a) and TEM (c) of Co-MOF, SEM (b) and TEM (d) of NH_2−Co-MOF.

A/RPUF), and the differences in thermal stability, flame retardancy, and insulation performance were compared with those of APP/RPPU and N−C/RPUF. The synergistic effect of NH_2−Co-MOF and APP, as well as their effect on the fire safety, thermal performance, and thermal insulation of RPUF composites were investigated.

2. EXPERIMENT

2.1. Materials. Co $(NO_3)_2{\cdot}6H_2O$ (99.0%), 2-methylimidazole (98.0%), 2-aminoterephthalic acid (NH_2−BDC, 98.0%), *N*,*N*-dimethylformamide (DMF, 99.8%), CH_3OH (AR, ≥99.5%) were obtained from Titan Scientific, Shanghai, China. Ammonium polyphosphate (APP) was acquired from Huasheng Chemical Reagent, Tianjin, China. Silicone oil was acquired from Dow Corning Co., Ltd., Shanghai, China. A33 (33% triethylenediamine solution) Polyether polyols and MDI were procured from Zhuolian Zhichuang Polymer Materials Technology, Changzhou, China. Dibutyltin dilaurate was acquired from Aladdin Technology, Shanghai, China. The deionized water (DI) was self-made.

2.2. Synthesis of Co-MOF. Co $(NO_3)_2{\cdot}6H_2O$ (1.437 g) and 2-methylimidazole (1.987 g) were each added in 60 mL of CH_3OH. After complete dissolution, the solutions were quickly mixed together and kept in reaction at room temperature for 24 h. After washing and filtering the precipitate CH_3OH, the precipitate was dried for 12 h at 80 °C.

2.3. Synthesis of NH_2−Co-MOF. NH_2−BDC (170 mg) was added to 70 mL of DMF and completely dissolved by ultrasound. Twenty mL of methanol solution in which 500 mg of Co $(NO_3)_2{\cdot}6H_2O$ has been dissolved was slowly added, and stirred magnetically for 0.5 h. The mixed solution was poured into a 200 mL PTFE lined autoclave and reacted at 100 °C for 4 h. The precipitate was collected by centrifugation after washing with CH_3OH. Then it was dried for 12 h at 80 °C.

2.4. Preparation of RPUF and Its Composites. The one-step method was used for the preparation of RPUF and composite RPUF. A certain amount of polyether polyol, DI (0.04 g), silicone oil (4 g), dibutyltin dilaurate (0.04 g), A33 (0.08 g), and flame retardant (1g Co-MOF or 1 g NH_2−Co-MOF or 1 g APP or 0.5 g NH_2−Co-MOF and 0.5 g APP) were added in a plastic beaker and stirred at a speed of 1000 rpm for 1 min. Then, MDI was added and stirred thoroughly for 1 min, and the foam was quickly poured into the mold and finally cured at room temperature for 24 h. The formulations of RPUFs are given in Table 1, and the synthesis scheme is illustrated in Figure 1.

2.5. Characterization. The morphology of the MOFs and dispersion of the MOFs in RPUF were studied by a Zeiss Sigma 300 scanning electron microscope (Carl Zeiss AG, Germany) at an acceleration voltage of 5 kV.

An Xi+ spectrometer (Thermo Fisher Scientific) was used for X-ray photoelectron spectroscopy (XPS) testing.

The crystal morphology of MOFs was tested by X-ray diffraction (XRD) using Cu Kα radiation at 40 kV and 15 mA on a Rigaku Smartlab X-ray diffractometer (Rigaku Corporation, Japan).

The Nicolet IS50 Fourier Transform Infrared spectrometer (FT-IR) was utilized for detecting the chemical structure of MOFs and char residual. The test wavenumber was between 400 and 4000 cm^{-1}.

Thermogravimetric analysis (TGA) (TGA/DSC 3+Stare System, Mettler-Toledo, Switzerland) and a Nicolet iS20 FTIR spectrometer (Thermo Fisher Scientific) were utilized for thermogravimetric analysis (TGA) and TGA-infrared spectroscopy (TG-IR) testing. The sample was heated from 30 to 700 °C under a nitrogen atmosphere.

The nitrogen adsorption isotherm of flame retardants was measured using the ASAP 2460 analyzer from MICROMERITICS Instruments in the United States using the BET method.

The microstructure of the MOFs was studied by using a JEM transmission electron microscope (TEM). Methanol is used for the dispersion and preparation of RPUF composite powder samples.

According to ISO standard 5660, a cone calorimeter was used to assess the sample's combustion characteristics. Under a heat flux of 35 $kW{\cdot}m^{-2}$. The sample used for testing was prepared in a size of 100 mm × 100 mm × 3 mm.

https://doi.org/10.1021/acsomega.4c08026
ACS Omega 2025, 10, 892−903

Raman spectra of the char residue were obtained by using a Renishaw (U.K.) Raman spectrometer at room temperature, scanning from 500 to 2000 cm^{-1}.

The thermal conductivity of RPUF and composite materials was tested by using a thermal viscoelasticity testing system. The samples are 75 mm × 15 mm cylinder.

3. RESULTS AND DISCUSSION

3.1. Characterization of MOFs. The SEM and TEM images of the MOFs are shown in Figure 2. The SEM and TEM images of Co-MOF are displayed in Figure 2a,c, while the SEM and TEM images of NH_2−Co-MOF are shown in Figure 2b,d. According to the SEM and TEM images of Co-MOF, it is evident that Co-MOF displays a dodecahedral shape with an average particle size of 500 nm. Based on the SEM and TEM images of NH_2−Co-MOF, graphene-like folds demonstrated the layered structure of NH_2−Co-MOF, aligning with previous studies reported in the literature.[32] The above results indicate that the microstructures of the synthesized MOFs meet expectations.

Figure 3 displays the XRD spectrum of MOFs. All characteristic peaks align with earlier studies,[33,34] confirming the successful crystal structures of Co-MOF and NH_2−Co-MOF.

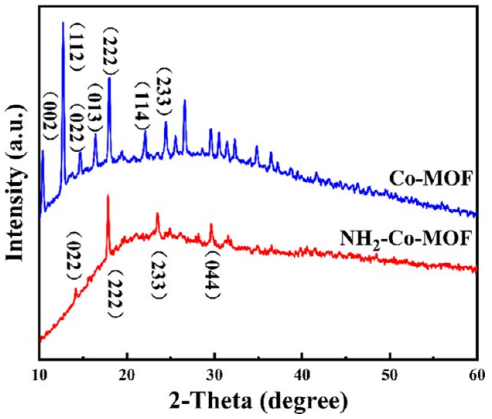

Figure 3. XRD spectra of the MOFs.

The synthesis of MOFs was demonstrated by XPS. As exhibited in Figure 4a, the binding energies at 284.8, 398.9, and 780.4 eV correspond to C 1s, N 1s, Co 2p, respectively, confirming that the chemical compositions of MOFs were achieved as intended. Figure 4b−e shows the XPS curves of Co 2p and N 1s of MOFs, respectively. Co ions have two characteristic peaks, indicating that Co ions have Co^{3+} and Co^{2+} ions, respectively, and there is a satellite peak near each main peak.[35] Furthermore, the N 1s spectrum was analyzed and fitted with three peaks representing pyridine nitrogen, graphitic nitrogen, and oxidized nitrogen, respectively.[36] The results indicate that no impurity elements were detected in the MOFs, and the chemical composition of the MOFs meets the design requirements.

The FT-IR spectra of MOFs are plotted in Figure 5. In the Co-MOF spectrum, the peak at 3430 cm^{-1} corresponds to the intramolecular association of the O−H bond. The peak at 2920 cm^{-1} is caused by the C−H stretching vibration. The C═N stretching vibration peak is located at 1631 cm^{-1}. The peaks at 1410, 1133, and 983 cm^{-1} are all caused by the vibration of the C−N bond. The peak at 1295 cm^{-1} is a tertiary amine nitrogen peak. The characteristic peak observed at 745 cm^{-1} is linked to the vibration of the imidazole ring, whereas the notable peak at 417 cm^{-1} results from the Co−N bond.[37] Besides, the spectrum of NH_2−Co-MOF is similar to the previous study.[34] The peak at 3361 cm^{-1} results from the stretching vibration of the $-NH_2$. The characteristic peak of C═O stretching vibration appears at 1676 cm^{-1}. −COO− asymmetric stretching vibration is marked by the peak at 1583 cm^{-1}. The bending vibration peak of C−H in CH_3 appears at 1442 cm^{-1}. The peaks at 1403 and 1258 cm^{-1} are associated with the symmetric stretching of −COO− and C−N−C bond vibration in the BDC linker, respectively.[35] The characteristic peaks of C−H in the BDC benzene ring appear at 868 and 793 cm^{-1}. The peak at 419 cm^{-1} originates from the stretching vibration of Co−N.

The results of BET are shown in Figure 6. The BET surface area of Co-MOF measures 1590.3 $m^2 \cdot g^{-1}$, featuring a total pore volume of 0.658 $cm^3 \cdot g^{-1}$, demonstrating a characteristic Type I hysteresis band.[31] The BET surface area for NH2-Co-MOF is 3.65 $m^2 \cdot g^{-1}$, with a total pore volume of 0.039 $cm^3 \cdot g^{-1}$. Its isotherm shows type III, usually representing macroporous materials without pores or with low adsorption energy.[38] The small surface area of NH_2−Co-MOF also confirms this feature.

Figure 7 shows the TAG and DTG curves of MOFs under N_2, with corresponding data presented in Table 2. $T_{5\%}$, $T_{10\%}$, and $T_{50\%}$ refer to the temperatures at which there is a thermal weight loss of 5, 10, and 50%, respectively. Meanwhile, T_{max} is defined as the temperature at which the rate of thermal weight loss is maximized. As shown in Figure 7a, the thermal weight loss of Co-MOF is slight until 300 °C, which might be due to the decomposition of residual solvent molecules, and this stage ends at 300 °C. In the DTG curves, the gradual decrease in the thermal decomposition rate after reaching 300 °C also indicates the end of this stage. The decomposition of Co-MOF begins at 300 °C. Before reaching 500 °C, the decomposition of Co-MOF is not severe, which might be due to the oxidation of cobalt complexes.[26] After reaching 500 °C, Co-MOF begins to decompose violently, and the residual amount at 700 °C (R_{700}) is 46.5 wt %. Compared with Co-MOF, the decomposition of NH_2−Co-MOF occurs earlier. Before 200 °C, residual solvent molecules undergo decomposition. At 200−315 °C, $-NH_2$ decomposes and generates NH_3, which is consistent with the trend of the DTG curves. The ligand portion of NH_2−Co-MOF begins to decompose at 350 °C and reaches its peak decomposition rate at 485 °C, with an R_{700} of 28.9 wt %. By comparing specific thermal decomposition parameters, the $T_{5\%}$, $T_{10\%}$, and $T_{50\%}$ of Co-MOF are much higher than those of NH_2−Co-MOF, indicating that Co-MOF has excellent thermal stability. However, the severe decomposition of NH_2−Co-MOF indicates that it contains a large number of nitrogen-containing groups, which are thermally decomposed and generate noncombustible gases such as NH_3, thereby diluting combustible gases.

3.2. Thermal Insulation Performance Testing of RPUF Composite Materials. Figure 8 illustrates the thermal conductivity of RPUF and its composites. Neat RPUF exhibits the lowest thermal conductivity, making it an effective thermal insulating material. The enhancement in thermal conductivity observed in the C/RPUF and A/RPUF samples is constrained by the thermal resistance at the interface between the filler and the matrix, resulting in increases of merely 6.6 and 7.8%, respectively. However, the thermal conductivity of N−C/

https://doi.org/10.1021/acsomega.4c08026
ACS Omega 2025, 10, 892−903

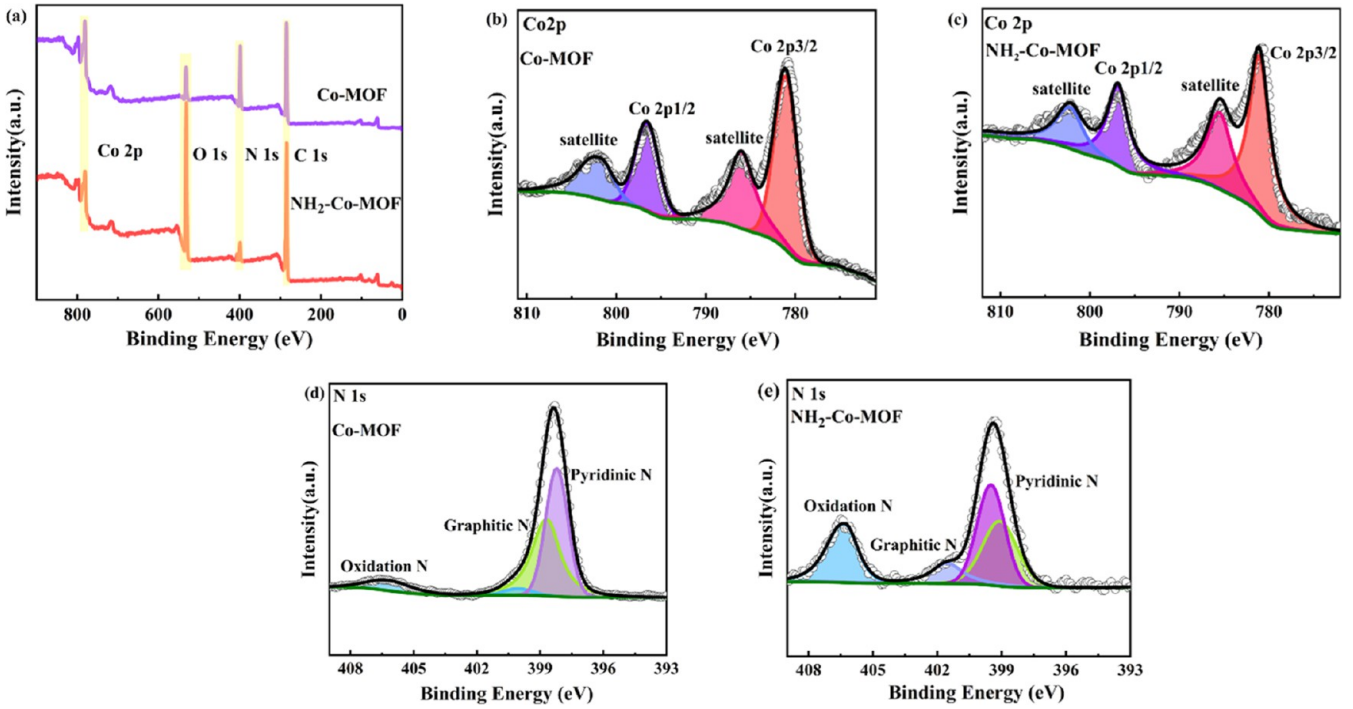

Figure 4. XPS spectra of MOFs. (a) Total spectrum, (b, c) Co 2p spectrum, and (d, e) N 1s spectrum.

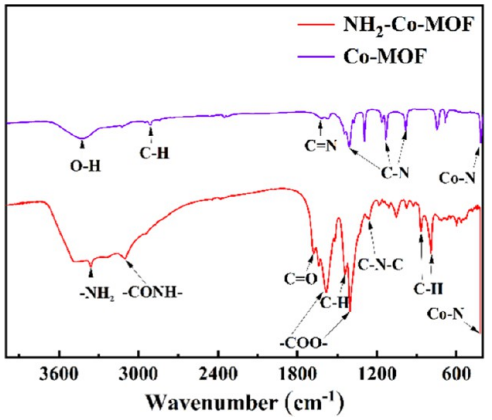

Figure 5. FT-IR results of the MOFs.

RPUF and N−C/A/RPUF samples increased by 10.2 and 12.0%, respectively. This may be due to the introduction of $-NH_2$ improving the dispersion of fillers in RPUF, thereby enhancing the interfacial interaction between flame retardant additives and the RPUF matrix.

3.3. Thermal Stability of RPUF Composites. Figure 9 displays the TGA and DTG curves for RPUF and its composites in N2, with corresponding data provided in Table 3. The decomposition of RPUF can be categorized into two primary stages. The initial stage occurs between 200 and 436 °C, mainly due to the breaking of polyurethane bonds and the thermal polymerization reaction of polyols.[35,36] The second stage occurs between 436 and 700 °C, which might be due to further condensation of RPUF. After addition of flame retardants, the thermal decomposition process of the matrix was not altered. However, the enhanced thermal conductivity and the catalytic dehydration effects of APP lead to a reduction in the $T_{10\%}$ of all RPUF composites.[39] In addition, the T_{max} of the composites is reduced compared to that of neat RPUF, confirming that the addition of flame retardants enhances the thermal decomposition and carbonization of RPUF composites. The addition of NH_2−Co-MOF and APP increases the R_{700} of RPUF from 14.6 to 16.1%, thereby benefiting the flame retardancy of RPUF composites.

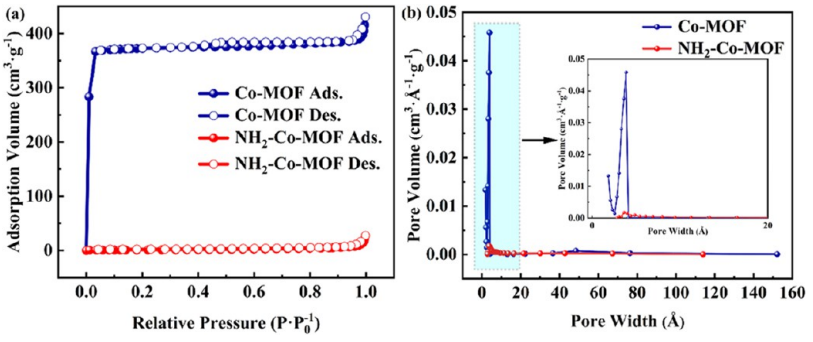

Figure 6. Results of BET. (a) N_2 adsorption−desorption isotherm and (b) pore size distribution.

https://doi.org/10.1021/acsomega.4c08026
ACS Omega 2025, 10, 892−903

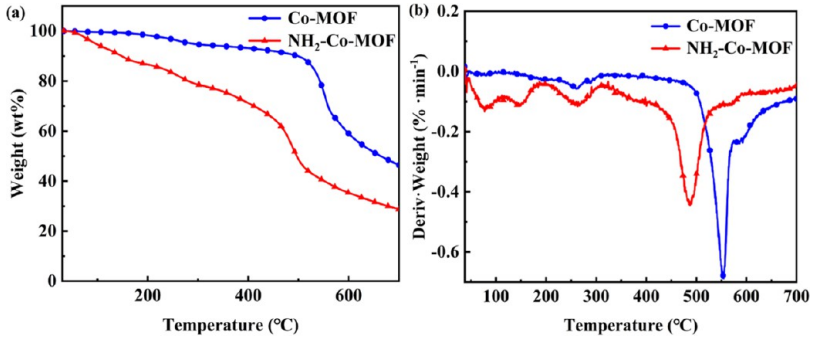

Figure 7. TGA results of MOFs under N_2. (a) TG, (b) DTG.

Table 2. TG and DTG Data of MOFs under N_2

sample codes	$T_{5\%}$/°C	$T_{10\%}$/°C	$T_{50\%}$/°C	T_{max}/°C	R_{700}/%
Co-MOF	288.3	498.9	663.8	554.6	46.5
NH_2-Co-MOF	95.9	148.3	496.6	487.3	28.9

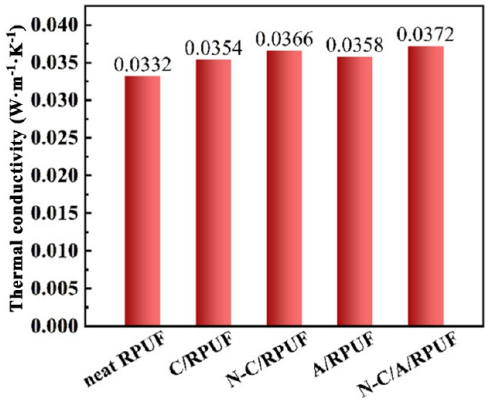

Figure 8. Thermal conductivity of RPUFs.

3.4. Dispersion of Flame Retardants in RPUF. The dispersion of additives in composite materials can affect their mechanical properties. In order to study the dispersion of flame retardants in composite materials, SEM was used to observe the dispersion of flame retardants in RPUF, as shown in Figure 10. Figure 10a,b−g,h are SEM and EDS images of C/RPUF, N−C/RPUF, A/RPUF, and N−C/A/RPUF, respectively. According to the EDS results, cobalt and phosphorus elements were detected in the corresponding samples, indicating the presence of flame retardants in the composite material. In the SEM images, the flame retardants are uniformly distributed without significant agglomeration and the flame retardants are effectively dispersed in the RPUF matrix.

Table 3. TG and DTG Data of RPUFs under N_2

sample codes	$T_{5\%}$/°C	$T_{10\%}$/°C	$T_{50\%}$/°C	T_{max}/°C	R_{700}/%
neat RPUF	330.7	350.2	415.3	413.9	14.6
C/RPUF	309.1	332.8	406.1	397.4	15.5
N−C/RPUF	297.1	321.5	400.5	405.9	15.7
A/RPUF	329.5	349.1	412.2	403.7	17.8
N−C/A/RPUF	295.5	321.4	398.7	394.3	16.1

3.5. Flame Retardancy Assessment. Figure 11 displays some parameters related to combustion behavior of RPUF and its composites. Figure 11a displays the pHRR curves of RPUF and its composites. The value of the pHRR of neat RPUF is 683.400 kW·m^{-2}. After adding flame retardants, the pHRR values of RPUF composites reduce. The pHRR value of N−C/RPUF is lower than that of C/RPUF, which is 649.785 kW·m^{-2}, indicating that the introduction of $-NH_2$ contributes to further reducing the pHRR. Compared to neat RPUF, the pHRR value of N−C/A/RPUF (529.7 kW·m^{-2}) decreases 22.5%, indicating the synergistic effect of NH_2−Co-MOF and APP. In Figure 11b, the THR curves show the same trend as HRR. The THR value of N−C/A/RPUF is the lowest (55.250 MJ·m^{-2}), which is 37.4% lower than that of neat RPUF (88.305 MJ·m^{-2}). The above results indicate that the synergistic effect of NH_2−Co-MOF and APP can maximize the flame retardant performance of RPUF.

The large amount of smoke generated by a fire may cause casualties. Figure 11c,d show the smoke production rate (SPR) and total smoke production (TSP) curves of the RPUFs. During the combustion process of the APP, a significant quantity of gas is generated, which explains why the peak smoke production rate (pSPR) value of A/RPUF (0.240 m^2·

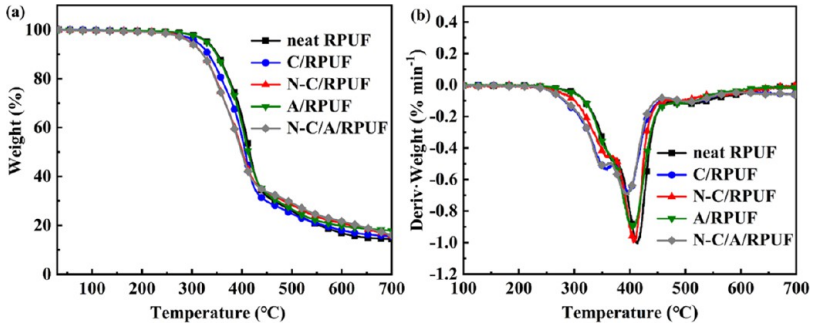

Figure 9. TGA results of RPUF under N_2. (a) TG, (b) DTG.

https://doi.org/10.1021/acsomega.4c08026
ACS Omega 2025, 10, 892−903

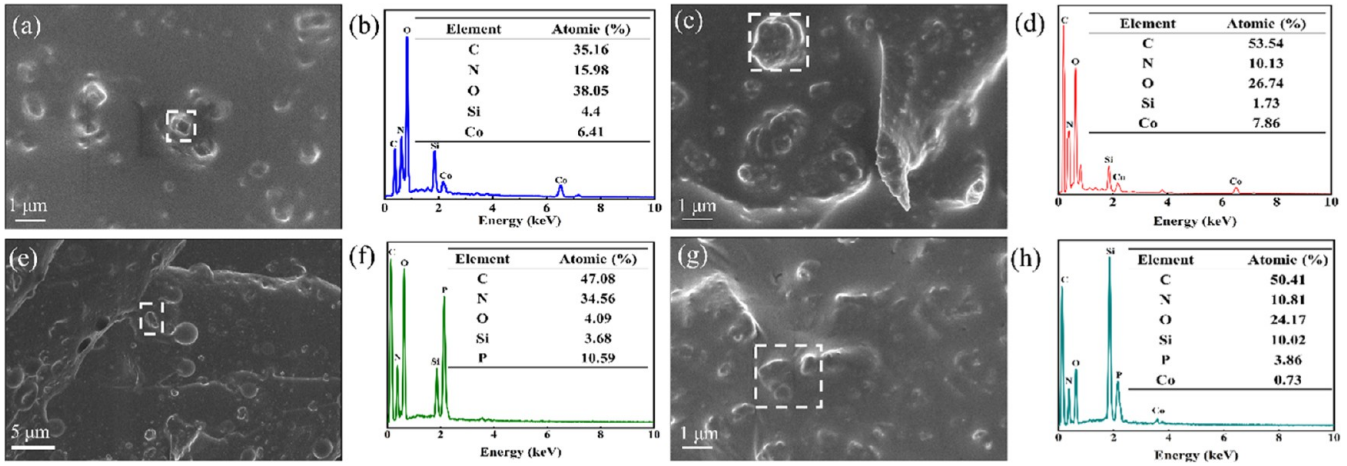

Figure 10. SEM and EDS images of RPUF composites. (a, b) C/RPUF, (c, d) N−C/RPUF, (e, f) A/RPUF, and (g, h) N−C/A/RPUF.

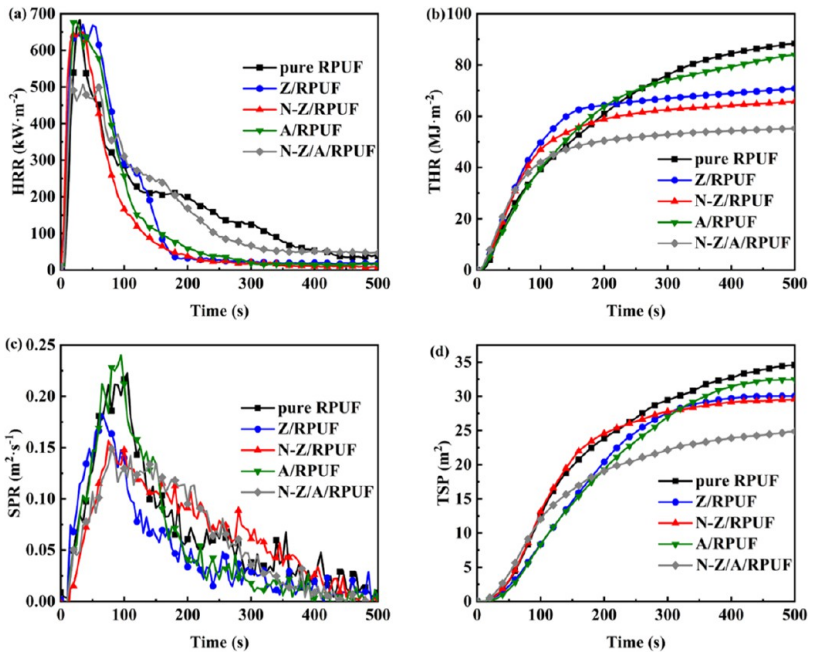

Figure 11. Results of cone calorimetry tests of the RPUF. (a) HRR curves, (b) THR curves, (c) SPR curves, (d) TSP curves.

Table 4. Comparison of the Parameter Decrease Rate in RPUF Cone Calorimeter Test with Different MOFs as Flame Retardants Added

samples	content of additive (wt %)	pHRR (%)	THR (%)	pSPR (%)	TSP (%)	references
N−C/A	2	22.5	37.4	33.2	28.1	this work
ZIF-7	12	17	19.2			30
ZIF-8	12	17	33.9			30
ZIF-11	12	17	21.3			30
A@P-Z	10	38.6	45.9	19.2	53.4	31
C-MOF-MWCNTs	4.5	23.0	12.3	26.0	11.7	41

s^{-1}) is higher than that of neat RPUF (0.223 $m^2 \cdot s^{-1}$). The pSPR value of N−C/A/RPU (0.149 $m^2 \cdot s^{-1}$) is the lowest, which decreases 33.2%. By the addition of flame retardants, the TSP value of RPUF composites decreased. The TSP value of N−C/A/RPUF (24.86 m^2) is the lowest, which reduces 28.1%. Therefore, flame retardants will be beneficial for individuals trying to flee from a fire.

Table 4 compares the decrease rate of cone calorimeter parameters for RPUF composites prepared with N−C/A and other MOFs as flame retardants.

3.6. Char Residue Analysis. The structure of the char residue significantly enhances the flame retardancy of condensed phases. A systematic study was detected on the structure, elemental composition, and degree of graphitization of the char residue after a cone calorimeter test to understand the effect of flame retardants on the carbonization process.

https://doi.org/10.1021/acsomega.4c08026
ACS Omega 2025, 10, 892−903

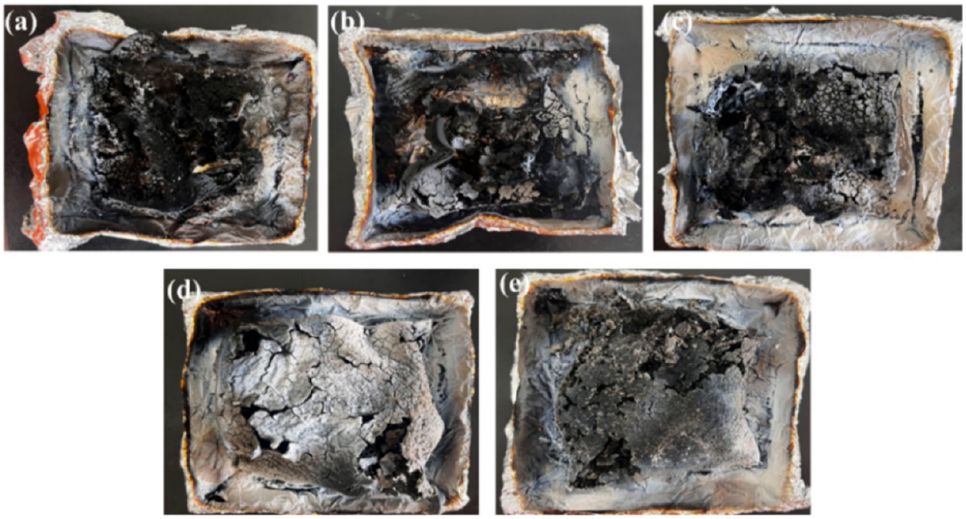

Figure 12. Digital images of char residue for (a) neat RPUF, (b) C/RPUF, (c) N−C/RPUF, (d) A/RPUF, and (e) N−C/A/RPUF.

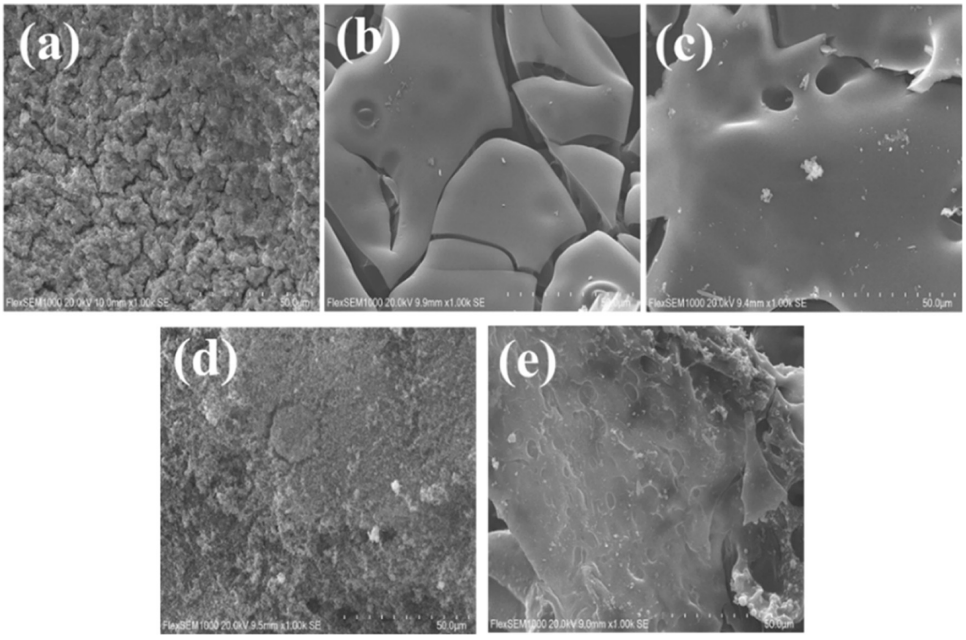

Figure 13. SEM images of the char residue: (a) neat RPUF, (b) C/RPUF, (c) N−C/RPUF, (d) A/RPUF, (e) N−C/A/RPUF.

Digital images of the char residue are displayed in the Figure 12, and Figure 13 showed the SEM images of the char residue. It is obvious that the neat RPUF sample burned very thoroughly, and the char residue does not have a complete structure. Its microstructure also shows a large number of pores, which provides adequate space for the transfer of heat and combustibles both inside and outside the matrix throughout the combustion process. It also accelerates erosion of the matrix by the external environment. The char residue and integrity of the C/RPUF and N−C/RPUF samples have been improved, but the microstructure still shows a significant quantity of pores. The addition of the APP significantly improves the char residue and integrity of the sample and exhibits an expanded structure. Compared with A/RPUF, the SEM image of the N−C/A/RPUF sample shows a denser and more continuous carbon layer, which can effectively prevent heat and mass transfer, thereby protecting the substrate from erosion.

The elemental composition of the char residue was detected by XPS. In Figure 14a, the char residue of neat RPUF consists of C and O elements. The char residue of N−C/A/RPUF contains C, N, O, Co, and P elements. Figure 14b−f displays Co 2p, P 2p, N 1s, C 1s, and O 1s high-resolution XPS spectra of the char residue of N−C/A/RPUF, respectively. The Co 2p peaks are observed at 797.1 and 781.3 eV, indicating the formation of Co_3O_4. The presence of satellite peaks confirms that Co-MOF has been transformed into porous oxidized nano cobalt.[37] According to previous literature reports, the presence of Co_3O_4 enhances char layer stability and significantly suppresses flue gas emissions.[40] The two peaks of P 2p represent P−O and Co−P bonds, indicating the presence of phosphate and H_3PO_4 in the char residue. On the one hand, PO_4^{3-} can catalyze the formation of the char layer, and the generated phosphorus oxide can also enhance the continuity of the char layer. On the other hand, H_3PO_4 decomposes and absorbs heat, lowering the temperature and thus delaying

https://doi.org/10.1021/acsomega.4c08026
ACS Omega 2025, 10, 892−903

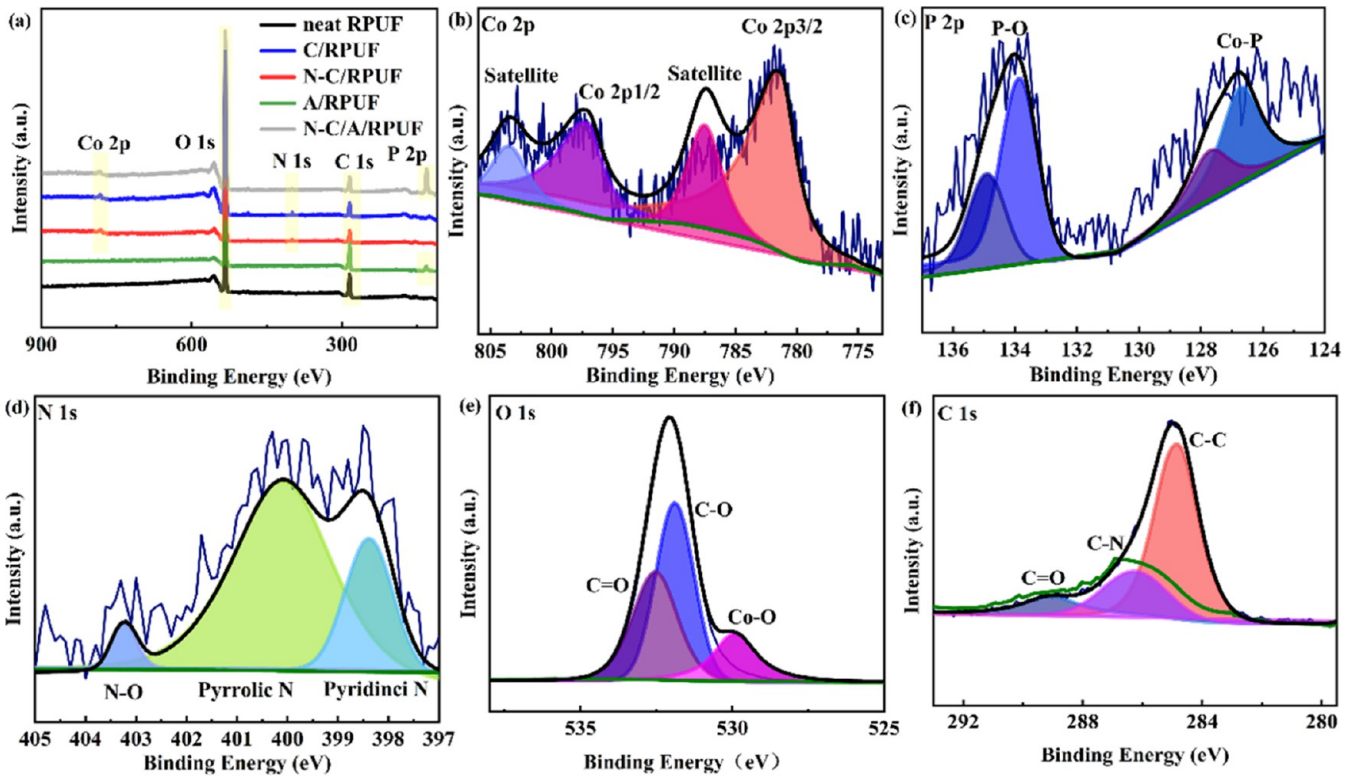

Figure 14. XPS results of the char residue. (a) Total XPS spectrum, (b–f): Co 2p, P 2p, N 1s, O 1s, and C 1s spectra of N–C/A/RPUF.

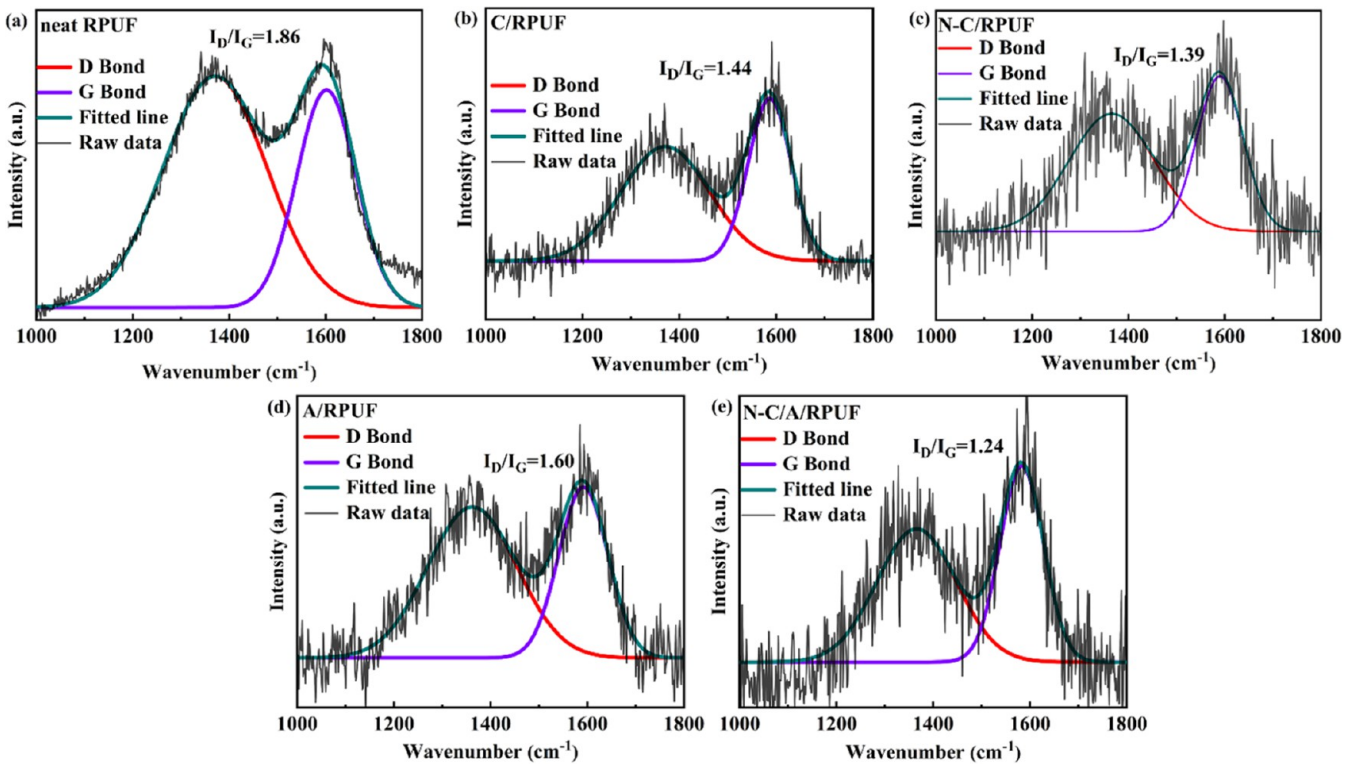

Figure 15. Raman spectra of the char residue. (a) Neat RPUF, (b) C/RPUF, (c) N–C/RPUF, (d) A/RPUF, and (e) N–C/A/RPUF.

combustion. In addition, H_3PO_4 decomposes to generate $PO^{\cdot}$ that can capture $H^{\cdot}$ and can fundamentally prevent combustion.

The graphitization degree of the char residue is evaluated by using the Raman spectrum. The D bonds and G bonds, located approximately at 1350 and 1580 cm^{-1}, correspond to the vibrations associated with disordered carbon and graphitic carbon, respectively. In Figure 15, the lower the I_D/I_G value of the peak intensity ratio, the higher the degree of graphitization is. After adding flame retardants, the I_D/I_G values decrease,

https://doi.org/10.1021/acsomega.4c08026
ACS Omega 2025, 10, 892–903

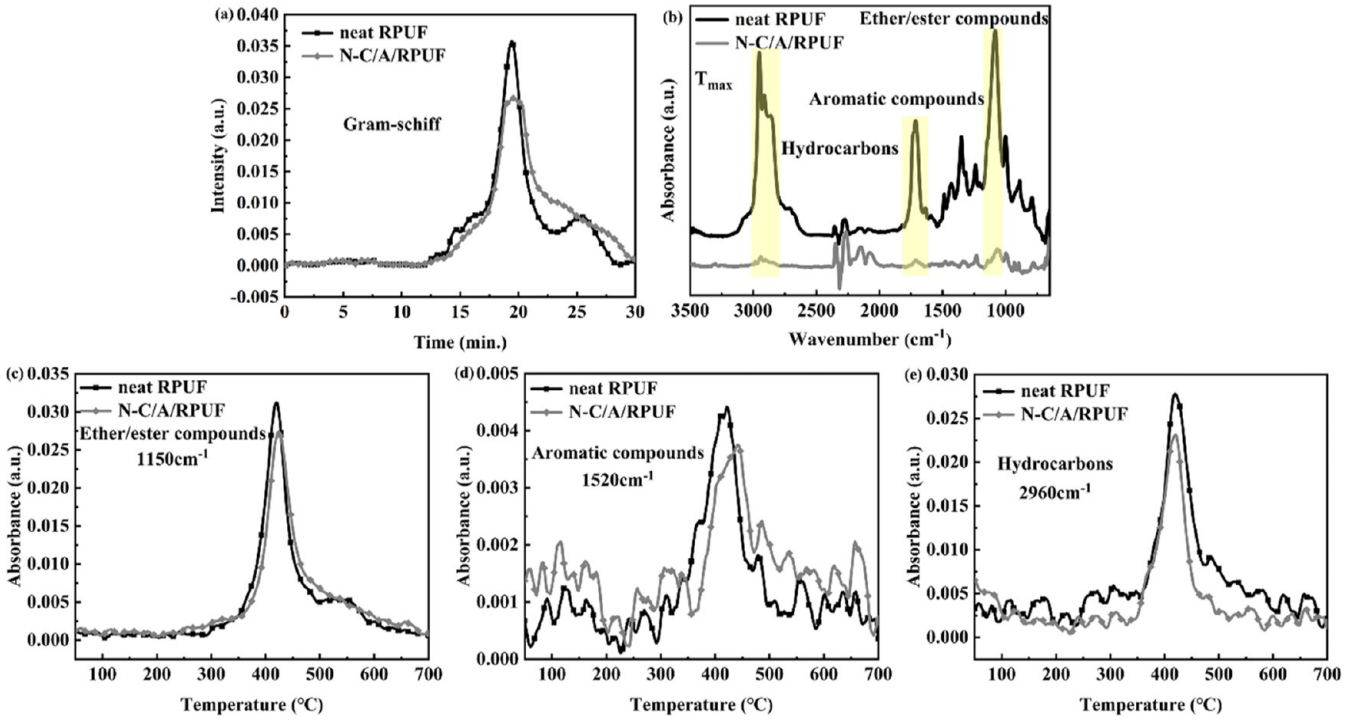

Figure 16. TG-IR results of neat RPUF and N−C/A/RPUF. (a) Gram-schiff curves, (b) the pyrolysis gaseous products at the T_{max}, (c−e) ethers, aromatic compounds, and hydrocarbon release profiles.

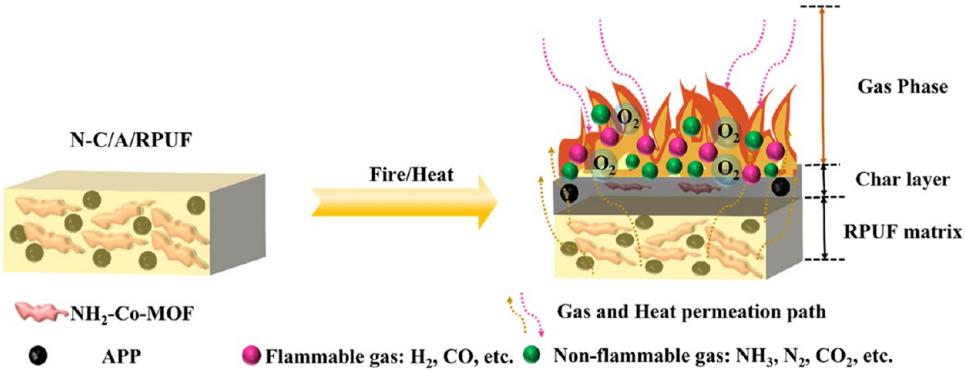

Figure 17. Schematic diagram of the flame retardancy mechanism.

indicating an improvement in the thermal stability of the char residue, which provides a sufficient barrier effect to suppress heat and mass transfer and smoke. With the addition of flame retardants, the I_D/I_G values of the composites char residue layer decreased. Among them, the I_D/I_G value of N−C/A/RPUF is the lowest, at 1.24, indicating that the char residue exhibits the greatest level of graphitization, and the char residue layer is uniform and stable, which enhances its barrier effect.

3.7. Characterization of Gaseous Products from Pyrolysis. A TG-IR test was used to identify the gaseous products during the combustion of RPUF composites. Figure 16 displayed the results of the TG-IR test. As shown in Figure 16a, compared to neat RPUF, the peak intensity of the N−C/A/RPUF sample significantly decreases, indicating that the synergistic effect of NH_2−Co-MOF and APP can decrease the overall volatile matter released during the decomposition of RPUF. The FT-IR curves of the pyrolysis gaseous products of RPUF composites at T_{max} are shown in Figure 16b. The neat RPUF and N−C/A/RPUF samples exhibit the similar thermal decomposition products, except that the peak intensity of neat RPUF is much higher than that of the N−C/A/RPUF sample.

With the purpose of further investigating the effect of NH_2−Co-MOF and APP on the release of gaseous products, the changes of peaks near 1150, 1520 and 2960 cm^{-1} in the FT-IR curve (corresponding to ether/ester compounds, aromatic compounds, and hydrocarbons, respectively) at different temperatures were analyzed, as illustrated in Figure 16c−f. The peak intensity of the N−C/A/RPUF sample decreases significantly, indicating that the synergistic effect of NH_2−Co-MOF and APP can significantly inhibit the release of pyrolysis products.

3.8. Flame Retardancy Mechanisms. Integrating the TG-IR, Raman, XPS, and SEM findings, Figure 17 illustrated the flame retardant mechanism of the synergy of NH_2−Co-MOF and APP on flame retardancy. Among all RPUF samples, N−C/A/RPUF exhibits the most effective flame retardancy and smoke suppression due to the synergistic use of NH_2−Co-MOF and APP. Specifically, NH_2−Co-MOF and APP generated substances such as Co_3O_4 and H_3PO_4 at high

https://doi.org/10.1021/acsomega.4c08026
ACS Omega 2025, 10, 892−903

temperatures. These substances not only catalyze the formation of char but also make the char layer more complete and more dense, thus better functioning as a barrier to prevent oxygen and heat transferring into the RPUF. At the same time, NH_2−Co-MOF and APP release noncombustible gases at high temperatures, including NH_3, N_2, CO_2, H_2O, phosphorus containing gases, etc. These gases reduce the levels of oxygen and flammable gases, thereby delaying the combustion behavior of the substrate. In addition, the APP generates $PO^{\cdot}$ radicals during the combustion process, which can capture $H^{\cdot}$ radicals, thereby inhibiting the combustion chain reaction and preventing combustion.

4. CONCLUSIONS

In this study, the NH_2−Co-MOF is synthesized by a hydrothermal method, and RPUF flame retardant composites containing NH_2−Co-MOF and APP are prepared by a one-step method. The thermal stability, flame retardancy, and thermal insulation of RPUF composites as well as the synergistic effect of NH_2−Co-MOF and APP on flame retardant RPUF are investigated. The conclusions are as follows:

(1) The SEM image shows the graphene-like structure of NH_2−Co-MOF. The XRD results indicate that NH_2−Co-MOF has a good crystal structure. The XPS results confirm the absence of impurity elements. The FT-IR results also confirm the presence of characteristic structure such as Co−N bonds. The above results demonstrate the successful synthesis of NH_2−Co-MOF.

(2) The TGA results show that the R_{700} of neat RPUF was 14.6%, and the R_{700} of N−C/RPUF, A/RPUF, and N−C/A/RPUF increase to 15.7, 17.8, and 16.1%, respectively, indicating that the addition of flame retardants promotes carbonization of the composites, and improving its flame retardancy. The lower R_{700} of N−C/A/RPUF compared to A/RPUF is caused by the decomposition of N-containing groups in NH_2−Co-MOF, but this also helps to improve the fire safety of the composites by generating nonflammable gases.

(3) The cone calorimeter test results show that neat RPUF rapidly burned and generated a large amount of heat and smoke, and the pHRR and pSPR values of 683.400 kW·m^{-2} and 0.223 $m^2 \cdot s^{-1}$, respectively. Compared with neat RPUF, RPUF composites exhibit excellent fire safety and smoke suppression. Among these, N−C/A/RPUF demonstrates superior flame retardancy and smoke suppression, exhibiting pHRR and pSPR values of 529.7 kW·m^{-2} and 0.149 $m^2 \cdot s^{-1}$, respectively.

(4) Further speculation is made on the flame retardancy mechanism of the synergistic effect of NH_2−Co-MOF and APP by conducting SEM, XPS, Raman, and TG-IR tests on the char residue after cone calorimeter testing. According to the SEM image, numerous cracks and pores were detected in the char residue of neat RPUF. The addition of flame retardants can reduce the number of cracks and holes. The char residue of N−C/A/RPUF is dense and continuous, which can provide an excellent barrier effect, and the results of Raman testing also prove this. The XPS results indicate that the char residue of N−C/A/RPUF contains Co oxides and PO_4^{3-}, which can catalyze the formation of high-quality carbon layers. The TG-IR results indicate that the generation of nonflammable gases such as NH_3 and N_2 plays a role in diluting combustible gases. Meanwhile, the substance containing P also plays a role in quenching the combustion chain reaction.

AUTHOR INFORMATION

Corresponding Author

Shujie Yuan − *School of Safety Science and Engineering, Anhui University of Science and Technology, Huainan, Anhui 232001, China; Key Laboratory of Safe and Effective Coal Mining, Ministry of Education, Huainan, Anhui 232001, China;* orcid.org/0000-0002-1192-5813; Email: yuansj@aust.edu.cn

Authors

Zijin Chen − *School of Safety Science and Engineering, Anhui University of Science and Technology, Huainan, Anhui 232001, China*

Xiaoxue Xu − *School of Safety Science and Engineering, Anhui University of Science and Technology, Huainan, Anhui 232001, China*

Complete contact information is available at: https://pubs.acs.org/10.1021/acsomega.4c08026

Author Contributions

Z.C.: Investigation, data curation, formal analysis, and writing−original draft preparation. S.Y.: Conceptualization, methodology, writing−review and editing, supervision, and funding acquisition. X.X.: Methodology, investigation.

Notes

The authors declare no competing financial interest.

ACKNOWLEDGMENTS

This work was supported by "Anhui Economic and Information Technology Innovation (WJXJG [2012] No.118)."

REFERENCES

(1) Henry, C.; Gondaliya, A.; Thies, M.; Nejad, M. Studying the suitability of nineteen lignins as partialpolyol replacement in rigid polyurethane/polyisocyanurate foam. *Molecules* **2022**, *27*, 2535.

(2) Srihanum, A.; Tuan Noor, M. T.; Devi, K. P.; et al. Low density rigid polyurethane foam incorporated with renewable polyol as sustainable thermal insulation material. *J. Cell. Plast.* **2022**, *58*, 485−503.

(3) Tao, J.; Yang, F.; Wu, T.; et al. Thermal insulation, flame retardancy, smoke suppression, and reinforcement of rigid polyurethane foam enabled by incorporating a P/Cu-hybrid silica aerogel. *Chem. Eng. J.* **2023**, *461*, No. 142061.

(4) Ma, Z.; Liu, X.; Xu, X.; et al. Bioinspired, highly adhesive, nanostructured polymeric coatings for superhydrophobic fire-extinguishing thermal insulation foam. *ACS Nano* **2021**, *15*, 11667−11680.

(5) Acuña, P.; Lin, X.; Calvo, M. S.; et al. Synergistic effect of expandable graphite and phenylphosphonic—aniline salt on flame retardancy of rigid polyurethane foam. *Polym. Degrad. Stab.* **2020**, *179*, No. 109274.

(6) Zhang, X.; Sun, S.; Liu, B.; et al. Synergistic effect of combining amino trimethylphosphonate calcium and expandable graphite on flame retardant and thermal stability of rigid polyurethane foam. *Int. J. Polym. Anal. Charact.* **2022**, *27*, 302−315.

(7) Ma, C.; Qiu, S.; Xiao, Y.; et al. Fabrication of fire safe rigid polyurethane foam with reduced release of CO and NO_x and excellent physical properties by combining phosphine oxide-containing hyper-

branched polyol and expandable graphite. *Chem. Eng. J.* **2022**, *431*, 1210−1219.
(8) Xu, B.; Zhao, S.; Shan, H.; et al. Effect of two boron compounds on smoke-suppression and flame-retardant properties for rigid polyurethane foams. *Polym. Int.* **2022**, *71*, 1210−1219.
(9) Chan, Y. Y.; Schartel, B. It takes two to Tango: Synergistic Expandable Graphite-Phosphorus Flame Retardant Combinations in Polyurethane Foams. *Polymers* **2022**, *14*, 2562.
(10) Akar, A.; Değirmenci, B.; Köken, N. Fire-retardant and smoke-suppressant rigid polyurethane foam composites. *Pigm. Resin Technol.* **2023**, *52*, 237−245.
(11) Wang, Z.; Li, X. Mechanical Properties and Flame Retardancy of Rigid Polyurethane Foams Containing SiO_2 Nanospheres/Graphene Oxide Hybrid and Dimethyl Methylphosphonate. *Polym.-Plast. Technol. Eng.* **2018**, *57* (9), 884−892.
(12) Liu, Y.; He, J.; Yang, R. The Synthesis of Melamine-Based Polyether Polyol and its Effects on the Flame Retardancy and Physical-Mechanical Property of Rigid Polyurethane Foams. *J. Mater. Sci.* **2017**, *52*, 4700−4712.
(13) Yuan, Y.; Yang, H.; Yu, B.; et al. Phosphorus and Nitrogen-Containing Polyols: Synergistic Effect on the Thermal Property and Flame Retardancy of Rogid Polyurethane Foam Composites. *Ind. Eng. Chem. Res.* **2016**, *55*, 10813−10822.
(14) Wang, J.; Xu, B.; Wang, X.; Liu, Y. A phosphorous-based bi-functional flame retardant for rigid polyurethane foam. *Polym. Degrad. Stab.* **2021**, *186*, No. 109516.
(15) Zhu, H.; Xu, S. Preparation of flame-retardant rigid polyurethane foams by combining modified melamine-formaldehyde resin and phosphorus flame retardants. *ACS Omega* **2020**, *5*, 9658−9667.
(16) Li, Y.; Tian, H.; Zou, W.; et al. Fabrication and properties of rigid polyurethane nanocomposite foams with functional isocyanate modified graphene oxide. *Polym. Compos.* **2020**, *41*, 5126−5134.
(17) Wang, X.; Kalali, E. N.; Xing, W.; Wang, D. Y. CO_2 induced synthesis of Zn-Al layered double hydroxide nanostructures towards efficiently reducing fire hazards of polymeric materials. *Nano Adv.* **2018**, *3*, 12−17.
(18) Duan, X.; Wang, H. Z.; Ji, Z. G.; et al. A novel metal-organic framework for high storage and separation of acetylene at room temperature. *J. Solid State Chem.* **2016**, *241*, 152−156.
(19) Hall, E. A.; Redfern, L. R.; Wang, M. H.; Scheidt, K. A. Lewis Acid Activation of a Hydrogen Bond Donor Metal-Organic Framework for Catalysis. *ACS Catal.* **2016**, *6* (5), 3248−3252.
(20) Chowdhuri, A. R.; Singh, T.; Ghosh, S. K.; et al. Carbon Dots Embedded Magnetic Nanoparticles @Chitosan @Metal Organic Framework as a Nanoprobe for pH Sensitive Targeted Anticancer Durg Delivery. *ACS Appl. Mater. Interfaces* **2016**, *8* (26), 16573−16583.
(21) Vaitsis, C.; Sourkouni, G.; Argirusis, C. Metal Organic Frameworks (MOFs) and ultrasound: A review. *Ultrason. Sonochem.* **2019**, *52*, 106−119.
(22) Nabipour, H.; Wang, X.; Song, L.; Hu, Y. Metal-organic frameworks for flame retardant polymers application: A critical review. *Composites, Part A* **2020**, *139*, No. 106113.
(23) Pan, Y.-T.; Zhang, Z.; Yang, R. The rise of MOFs and their derivatives for flame retardant polymeric materials: A critical review. *Composites, Part B* **2020**, *199*, No. 108265.
(24) Meng, W.; Wu, H.; Bi, X.; et al. Synthesis of ZIF-8 with encapsulated hexachlorocy-clotriphosphazene and its quenching mechanism for flame-retardant epoxy resin. *Microporous Mesoporous Mater.* **2021**, *314*, No. 110885.
(25) Xu, W.; Wang, X.; Wu, Y.; et al. Functionalized graphene with Co-ZIF absorbed birate ions as an effective flame retardant and smoke suppression agent for epoxy resin. *J. Hazard. Mater.* **2019**, *363*, 138−151.
(26) Hou, Y. B.; Hu, W. Z.; Gui, Z.; et al. Preparation of Metal-Organic Framework and Their Application as Flame Retardant for Polystyrene. *Ind. Eng. Chem. Res.* **2017**, *56* (8), 2036−2045.
(27) Xu, W.; Chen, R.; Wang, G. Design water-soluble phenolic/zeolitic imidazolate framework-67 flame retardant coating via layer-by-layer assembly technology: Enhanced flame retardancy and smoke suppression of flexiable polyurethane foam. *Polym. Degrad. Stab.* **2020**, *176*, No. 109152.
(28) Li, A. J.; Xu, W. Z.; Chen, R.; et al. Fabrication of zeolitic imidazolate frameworks on layered double hydroxidenanosheets to improve the fire safety of epoxy resin. *Composites, Part A* **2018**, *112*, 558−571.
(29) Chen, W.; Jiang, Y.; Qiu, R.; Xu, W.; Hou, Y. Investigation of UiO-66 as flame retardant and its application in improving fire safety of polystyrene. *Macromol. Res.* **2020**, *28* (28), 42−50.
(30) Cheng, J.; Ma, D.; Li, S.; et al. Preparation of zeolitic imidazolate frameworks and their application as flame retardant as smoke suppression agent for rigid polyurethane foams. *Polymers* **2020**, *12* (12), No. 347.
(31) Liu, X. Y.; Guo, P. Y.; Zhang, B. R.; Mu, J. A novel ternary inorganic-organic hybrid flame retardant containing biomass and MOFs for high-performance rigid polyurethane foam. *Colloids Surf., A* **2023**, *671*, No. 131625.
(32) Bakar, B.; Dik, G.; Ulu, A.; Ateş, B. Immobilization of Xylanase into Zeolitic Imidazolate Framework-67 (ZIF-67) and Manganese-Doped ZIF-67(Mn/ZIF-67): A Comparison Study. *Top. Catal.* **2024**, *67*, 698−713.
(33) Xu, Z. M.; Xing, W. Y.; Hou, Y. B.; et al. The combustion and pyrolysis process of flame-retardant polystyrene/cobalt-based metal organic frameworks (MOF) nanocomposite. *Combust. Flame* **2021**, *226*, 108−116.
(34) Wang, G.; Liu, J.; Yue, F.; et al. Dual enzyme electrochemiluminescence sensor based on in situ synthesis of ZIF-67@AgNPs for the detection of IMP in fresh meat. *LWT* **2022**, *165*, No. 113658.
(35) Abrori, S. A.; et al. Non-Enzymatic Electrochemical Detection for Uric Acid Based on a Glassy Carbon Electrode Modified With MOF-71. *IEEE. Sens. J.* **2021**, *21*, 170−177.
(36) Yang, Q.; Ren, S.; Zhan, Q.; et al. Selective separation of methyl orange from water using magnetic ZIF-67 composites. *Chem. Eng. J.* **2018**, *333*, 49−57.
(37) Wan, M.; Shi, C.; Qian, X.; et al. Metal-organic Framework ZIF-67 Functionalized MXene for Enhancing the Fire Safety of Thermoplastic Polyurethanes. *Nanomaterials* **2022**, *12*, 1142.
(38) Bigdeli, H.; Moradi, M.; Hajati, S.; et al. Cobalt terephthalate MOF-templated synthesis of porous nano-crystalline Co_3O_4 by the new indirect solid state thermolysis as cathode material of asymmetric supercapacitor. *Phys. E* **2017**, *94*, 158−166.
(39) Velencoso, M. M.; Batting, A.; Markwart, J. C.; et al. Molecular Firefighting—How Modern Phosphorus Chemistry Can Help Solve the Challenge of Flame Retardancy. *Angew. Chem., Int. Ed.* **2018**, *57* (33), 10450−10467.
(40) Wang, X.; Jin, B.; Feng, R.; et al. A robust core-shell silver soot oxidation catalyst driven by Co_3O_4: Effect of tandem oxygen delivery and Co_3O_4-CeO_2 synergy. *Appl. Catal., B* **2019**, *250*, 132−142.
(41) Bo, G.; Xu, X.; Tian, X.; Yan, J.; Su, X.; Yan, Y. Bio-Based Rigid Polyurethane Foams Modified with C-MOF/MWCNTs and TBPBP as Building Insulation Materials: Synergistic Effect and Corresponding Mechanism for Enhancing Fire and Smoke Safety. *Polymers* **2022**, *14*, 3630.

https://doi.org/10.1021/acsomega.4c08026
ACS Omega 2025, 10, 892−903